Finite-Time Feedforward Decoupling and Precise Decentralized Control for DC Microgrids Towards Large-Signal Stability

Chuanlin Zhang, *Member, IEEE*, Xiaoyu Wang, *Student Member, IEEE*, Pengfeng Lin, *Student Member, IEEE*, Peter Xiaoping Liu, *Fellow, IEEE*, Yunda Yan, *Member, IEEE*, Jun Yang, *Senior Member, IEEE*

***Abstract*—This study is initiated by considering an emerging practical issue that DC microgrids should be able to operate with a large-signal stability sense when feeding both resistive loads and constant power loads (CPLs). To be more specific, the stability should be ensured in the presence of large variations of integrated renewable sources and CPLs, system internal uncertainties, external disturbances, coupled interactions, and other adverse effects. From a control point of view, we intentionally propose a general solution to realize the exact decentralized tracking control task for interconnected systems. Firstly, an alternative finite-time feedforward decoupling mechanism is presented, which is essentially different from existing design approaches via feedback domination or recursive cancellation processes. Secondly, a composite controller can be straightforwardly built from the system information since it is detached from stability analysis. One major advantage of the proposed design framework is that it reduces the design complexity and therefore facilitates the practical implementations. As a direct application, a simple decentralized composite controller is constructed for an autonomous DC microgrid system. Both numerical simulation and experimental comparison results show that a large-signal stability is achieved for DC microgrids under a range of different situations.**

***Index Terms*—DC microgrid, nonlinear interconnected system, large-signal stability, decentralized control, composite control.**

I. Introduction

DC microgrids have drawn extensive research attentions in recent decades [1]. Compared to a traditional AC microgrid, a DC microgrid possesses some unique advantages such as higher efficiency, more natural interface to various types of renewable energy source (RES) and energy-storage system (ESS), and better compliance with consumer electronics. Besides, the DC microgrid could avoid some troublesome problems in its AC counterpart, including reactive power flow, synchronization, and frequency regulation. It is well acknowledged that accurate power sharing and fast DC bus regulation are two essential requirements. Generally, droop control, derived from synchronous generator, provides a flexible method to allocate the power to different DC sources [2]. The output power of dispatchable units (DUs) can be proportional to their corresponding ratings. Notably, this droop method is typically decentralized and no communication across the entire DC system is needed.

Besides conventional resistive loads, it is noted that power electronic converters and motor drives in advanced automotive systems, when tightly regulated, behave as constant power loads (CPLs). As reported in [3], they always show negative impedance characteristics at input terminals, which might affect power quality and even lead to unstable situations. Hence, various active control techniques have been investigated to mitigate the instability problems caused by CPLs [4]. Furthermore, the high frequency characteristics of the switching power supply will increase the current/voltage rate of change and thus lead to electrical interactions. In this regard, multiple converters (especially DC-DC converters) usually produce adverse coupled interactions at the system level. These undesired interactions may result in global system instability, load imbalance for parallel converters, noise coupling and electromagnetic interference [5]. Hence it is widely regarded as a critical issue to maintain the stability for DC microgrids when facing the inevitable system uncertainties and disturbances [3], [4].

There are a variety of studies can be found in the literature to deal with the stabilization problem for DC microgrids, which mainly fall into two categories: small-signal analyses (SSA) and large-signal analyses (LSA) [6]. On the one hand, the principle of SSA is to calculate and locally linearize the system at the operating point. Then the stability can be studied via classical linear analysis tools, see, e.g., [7]–[9]. However, the small-signal model of the system will lose its accuracy if the operating condition is largely deviated, especially when plug-and-play (PnP) operation, RES fluctuations and load variations happen. On the other hand, LSA uses nonlinear tools, e.g., Lyapunov function based methods, to analyze the global system stability. It enables the system to resist large external

This work was supported in part by the Program for Professor of Special Appointment (Eastern Scholar) at Shanghai Institutions of Higher Learning, in part by the Natural Science Foundation of Shanghai (NO. 19ZR1420500), in part by the National Natural Science Foundation of China under the Grant 61573099 and 51607111, in part by Shanghai Science and Technology Innovation Action Plan and local Universities capacity building projects (NO.15160500800). *(Corresponding author: Peter Xiaoping Liu.)*

C. Zhang and X. Wang are with the Intelligent Autonomous Systems Lab, College of Automation Engineering, Shanghai University of Electric Power, Shanghai, China, 200090. (E-mail: clzhang@shiep.edu.cn; xywang@mail.shiep.edu.cn).

P. Lin is with the School of Interdisciplinary Graduate and the Energy Research Institute, Nanyang Technological University, 639798, Singapore (E-mail: linp0010@e.ntu.edu.sg).

P. X. Liu is with the Faculty of Mechanical Engineering and Automation, Zhejiang Sci-Tech University, Hangzhou, China and also with the Department of Systems and Computer Engineering, Carleton University, Ottawa ON, Canada (email: xpliu@sce.carleton.ca).

Y. Yan and J. Yang are with the Key Laboratory of Measurement and Control of CSE, Ministry of Education, School of Automation, Southeast University, Nanjing 210096, China. (E-mail: yd.yan@ieee.org, yyd@seu.edu.cn; j.yang84@seu.edu.cn).

disturbances caused by the reconnection/disconnection of DUs or the unpredictable variations of local/global loads. In [10], a composite nonlinear controller is proposed by integrating a nonlinear disturbance observer based on feedforward compensation with backstepping design algorithm. However, this controller would not be suitable for multi-source systems. Thereafter, a recent study in [11] develops a linear composite droop controller for DC microgrids, which only validates an input to state stability (ISS) property. Considering the size and cost of the large converter output capacitance, a virtual capacitor approach is proposed to increase the damping and improve the system stability margin in [12]. However, the amendment to the power reference value will result in undesirable performances on the mechanical loads. Two equivalent impedance estimation approaches, i.e., the Kalman filter and the recursive least squares method, are proposed in [13] to obtain more stable operating region. But the burdens of online computation will greatly grow with the increase of the system scale.

In this study, motivated by the decentralized control demand for the general DC microgrid system aiming to maintain the global system stability in the LSA sense, we will develop a novel finite-time feedfoward decoupling process and feedback domination control strategy for DC microgrids in autonomous operation mode. As a main difference with existing feedback control methods, we employ a composite control strategy including a feedforward compensation loop and a feedback control loop. To be specific, in each converter, a delicate designed observer is utilized to estimate the unknown lumped interactions between each DUs, external disturbances generated by variations of CPLs. Afterwards, the estimated lumped term are offset via finite-time feedforward decoupling processes. Notably, the proposed control strategy not only keeps the stability of the system under large disturbance cases, but also reduces the complexity of stability analysis. In the following sections, in order to maintain the theoretical justification of the proposed control strategy, we will also present a general solution for a class of general nonlinear interconnected systems. An explicit large-signal stability in terms of semi-global attractivity analysis is included. Then subsequently, as a real-life application of the proposed control theory, numerical simulation and experimental tests are provided to verify the effectiveness of the proposed design tools. It could be confident to reach that the proposed controller is able to stabilize the system towards a large-signal stability, and therefore providing a wider operating range for the DC microgrid system.

II. Problem Formulation of a Typical DC Microgrid

In this paper, we consider a typical multi-source autonomous DC microgrid as shown in Fig. 1(a), where the power electronic interfaces are boost type converters as they are the most widely used in DC microgrid systems. To proceed with theoretical analysis, as depicted by Fig. 1(b), we treat the system into a simplified structure including n-th boost converters linked in a parallel with the DC bus, while the loads

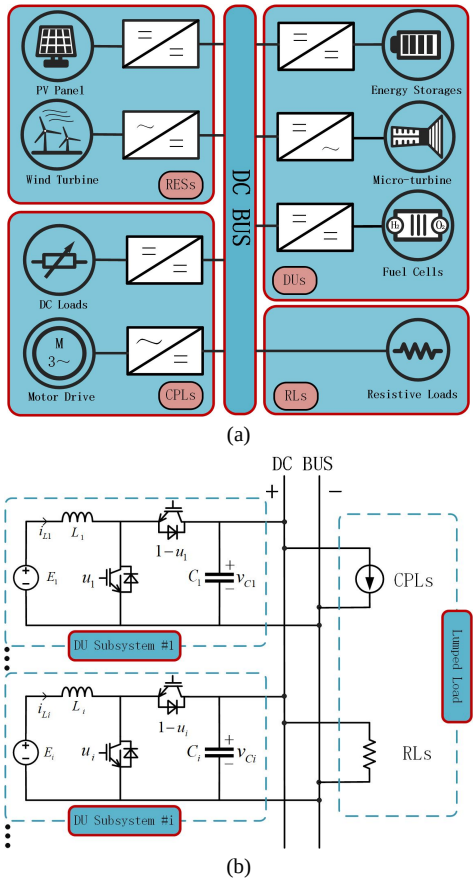

Fig. 1: A typical autonomous DC microgrid: (a) general layout, (b) simplified structure.

are categorized into a lumped resistive load R and a lumped CPL P_{CPL}. The governing equations for the i-th converter can be given as follows

$$\begin{cases} L_i\dot{i}_{Li} = -(1-\mu_i)v_{Ci} + E_i, \\ C_i\dot{v}_{Ci} = (1-\mu_i)i_{Li} - \frac{v_{Ci}}{R} - \frac{P_{CPL}}{v_{Ci}} \end{cases} \tag{1}$$

where L_i, C_i are the inductance and capacitance, respectively, i_{Li} and v_{Ci} are the instantaneous inductor current and capacitor voltage, μ_i is the duty cycle generated by the controller, E_i is the input voltage of each DC source. According to [14], we can transfer system (1) into a controllable canonical form via the following change of coordinates:

$$\begin{aligned} x_{i,1} &= 0.5L_i i_{Li}^2 + 0.5C_i v_{Ci}^2, \\ x_{i,2} &= E_i i_{Li}. \end{aligned} \tag{2}$$

Calculating the derivative of $x_{i,1}$ and $x_{i,2}$ yields

$$\begin{aligned} \dot{x}_{i,1} &= L_i i_{Li}\dot{i}_{Li} + C_i v_{Ci}\dot{v}_{Ci} = E_i i_{Li} - \frac{v_{Ci}^2}{R} - P_{CPL}, \\ \dot{x}_{i,2} &= \frac{E_i^2}{L_i} - \frac{E_i v_{Ci}}{L_i}(1-\mu_i). \end{aligned} \tag{3}$$

System (1) can also be rewritten as the following form

$$\begin{cases} \dot{x}_{i,1} = x_{i,2} + \Delta_{i,1}, \\ \dot{x}_{i,2} = u_i + \Delta_{i,2} \end{cases} \tag{4}$$

where $\Delta_{i,1} := -P_{CPL} - \frac{v_{Ci}^2}{R}$, $u_i := \frac{E_i^2}{L_i} - \frac{E_i v_{Ci}}{L_i}(1-\mu_i)$, $\Delta_{i,2}$ can be regarded as a lumped uncertainty term which consists of inevitable system internal uncertainties, external disturbances and unmodelled dynamics.

From the above analyses, it is concluded that the control objective can be transformed into designing a control signal u_i such that $x_{i,1}$ can track its reference x_{i1r} asymptotically, which is depicted by

$$\begin{aligned} x_{i1r} &= 0.5L_i i_{Lir}^2 + 0.5C_i v_{Cir}^2 \\ &= 0.5L_i \left(\frac{P_{CPL} + v_{Cir}^2/R}{E_i} \right)^2 + 0.5C_i v_{Cir}^2 \end{aligned} \quad (5)$$

where $v_{Cir} = V^* + m_i \Delta_{i,1}$ with V^*, m_i representing the nominal DC bus voltage and the droop coefficient for $i-th$ converter, respectively.

Up to now, one great hurdle appears: how to identify the two lumped terms, i.e., $\Delta_{i,1}$ and $\Delta_{i,2}$ in order to appoint a precise tracking objective v_{Cir} for each converter. By recalling that a classical double closed-loop PI control would result in a serious reaction delay and thereafter an adverse effect imposed on transient-time performance. Moreover, since linearized system control design may strongly limit the stability margin, where the system stability against a large CPL variation might deteriorate into breakdown. Upon on this well acknowledged fact, we will investigate a novel composite control strategy by integrating a finite-time feedforward decoupling procedure with a feedback control loop. To be specific, a fast convergent compensator should be added first to response immediately after the system operating condition is varied. Then a voltage feedback control loop could react rapidly to regulate the DC bus into a new voltage value owing to the droop effects. In order to present the result with theoretical justification, a general synthesis framework will be proposed in the following section.

III. General Theoretical Solution

A. General Interconnected System Depiction

Motivated by the practical control problem for DC microgrids, in this section, we address a general decentralized control problem for a class of m interconnected uncertain nonlinear systems of order n, depicted by

$$\begin{cases} \dot{x}_{i,j} = x_{i,j+1} + f_{i,j}(\bar{x}_{i,j}) + \Delta_{i,j}(t,\theta,x,d(t)),\ j \in \mathbb{N}_{1:n-1}, \\ \dot{x}_{i,n} = u_i + f_{i,n}(x_i) + \Delta_{i,n}(t,\theta,x,d(t)), \\ y_i = x_{i,1},\ i \in \mathbb{N}_{1:m} \end{cases} \quad (6)$$

where $\bar{x}_{i,j} = (x_{i,1}, x_{i,2}, \cdots, x_{i,j})^\top \in \Re^j$, $x_i = \bar{x}_{i,n} \in \Re^n$, $i \in \mathbb{N}_{1:m}$ [1], $x = (x_1^\top, x_2^\top, \cdots, x_m^\top)^\top \in \Re^{nm}$ are the system partial and full state vectors, u_i is the decentralized control input, $f_{i,j}(\cdot)$ is a known smooth nonlinear function, $d(t)$ is an external disturbance vector which is practically bounded, θ is the system uncertain time-varying parameter vector and its boundary is assumed to be known, $\Delta_{i,j}(\cdot)$ represents a lumped interaction term satisfying $\Delta_{i,j}(\cdot) \in \mathcal{C}^{n-j}$ [2] and $-\mathcal{D}_{i,j}^- \le \frac{\partial^s \Delta_{i,j}(\cdot)}{\partial t^s} \le \mathcal{D}_{i,j}^+$ with two known positive constants $\mathcal{D}_{i,j}^+$ and $\mathcal{D}_{i,j}^-$ for $i \in \mathbb{N}_{1:m}, j \in \mathbb{N}_{1:n}$, $s \in \mathbb{N}_{1:n-j+1}$. The output reference signal for $i-$th subsystem is denoted by y_{ri} whose $n-$th order derivative are assumed to be piecewise continuous, known and bounded.

Regarding the decentralized control issue for system (6), there are numerous results devoted to solve the stabilization problem based on certain assumptions and synthesis tools. On one hand, backstepping based decentralized control methods are widely employed, see e.g., [15], [16]. Prior to carrying out the recursive design approaches, the nonlinear interactions of the system are normally assumed to be presented in a weakly coupled form, see for instance, a form expressed by $\Delta_{i,j}(y_1, y_2, \cdots, y_m, x_i)$ is commonly seen in [17]–[19] and references therein. While these assumptions look fine, they may not be well satisfied in many practical interconnected systems, such as the DC microgrid system operating under a droop control mode [5]. Moreover, with the increase of system order, the controller form is also expanding, making it too complex to be realized. On the other hand, aiming at relaxing the interaction requirement and simplify the control expression, the feedback domination control method is proved to be an effective systematic design tool for interconnected systems even when the system is presented with strongly coupled interactions [20], [21]. However, it should be pointed out that, as a common feature of the domination based approaches, a nonlinearity growth condition is essentially required and the presence of uncertainties and disturbances could be a hurdle to employ the domination strategy. For a wide range of interconnected systems (6), it is still very challenging to realize the exact decentralized tracking objective due to the presence of both unknown strongly coupled interactions and external mismatched disturbance.

A typical manner in the literature to get around the problem is to impose certain assumptions on the interaction terms such that either cancellation or domination strategies can be used. If we look back all the control strategies employed to deal with the interactions which are strongly coupled with unknown disturbances, it seems to be clear that a global exact decentralized tracking objective is too ambitious and is obviously impossible via only feedback control loops. Inspired by recent composite control design approaches [22], [23], based on a semi-global control objective, we will present a novel decentralized control algorithm by integrating a finite-time feedforward decoupling process and a feedback domination control strategy. To this aim, a higher-order sliding mode (HOSM) observer is first employed to enable a precise finite-time feedforward compensation. Secondly, a non-recursive synthesis manner based on a semi-global stability criterion is proposed to achieve an exact decentralized tracking task. Then a rigorous stability analysis is provided to guarantee the semi-global stability and local convergence.

[1] $\mathbb{N}_{j:i} := \{j, j+1, \cdots, i\}$ with integers j and i satisfying $0 \le j \le i$.

[2] the symbol $\mathcal{C}^i$ denotes the set of all differentiable functions whose first $i-$th time derivatives are continuous

B. Decentralized Controller Design

Recalling that $\Delta_{i,j}(\cdot) \in \mathcal{C}^{n-j}$, we first construct the following higher-order sliding mode observer to estimate the lumped term $\Delta_{i,j}(\cdot)$ and its $n-j+1$-th derivatives [24]

$$\begin{cases} \dot{z}_{i,j,0} = \hbar_{i,j,0} + x_{i,j+1} + f_{i,j}(\bar{x}_{i,j}), \\ \hbar_{i,j,0} = z_{i,j,1} - l_{i,j,0}\lambda_{i,j}^{\alpha_{i,j,0}} \lfloor z_{i,j,0} - x_{i,j} \rceil^{1-\alpha_{i,j,0}}, \\ \dot{z}_{i,j,1} = \hbar_{i,j,1}, \\ \quad \vdots \\ \dot{z}_{i,j,k} = \hbar_{i,j,k}, \ k \in \mathbb{N}_{1:n-j+1}, \\ \hbar_{i,j,s} = z_{i,j,s+1} - l_{i,j,s}\lambda_{i,j}^{\alpha_{i,j,s}} \lfloor z_{i,j,s} - \hbar_{i,j,s-1} \rceil^{1-\alpha_{i,j,s}}, \\ s \in \mathbb{N}_{1:n-j}, \\ \hbar_{i,j,n-j+1} = -l_{i,j,n-i+1}\lambda_{i,j}^{\alpha_{i,j,n-j+1}} \\ \qquad \times \lfloor z_{i,j,n-j+1} - \hbar_{i,j,n-j} \rceil^{1-\alpha_{i,j,n-j+1}} \\ j \in \mathbb{N}_{1:n}, \ i \in \mathbb{N}_{1:m} \end{cases} \tag{7}$$

where $x_{i,n+1} = u_i$, $\alpha_{i,j,s} = \frac{1}{n+2-j-s}$, $l_{i,j,s} \in \Re_+$, $\lambda_{i,j} \in \Re_+$ are auxiliary design parameters, $z_{i,j,0} = \hat{x}_{i,j}$, $z_{i,j,1} = \widehat{\Delta}_{i,j}$, $z_{i,j,s} = \widehat{\Delta_{i,j}^{(s-1)}}$ represent the estimates of $x_{i,j}$, $\Delta_{i,j}$ $\Delta_{i,j}^{(s-1)}$, respectively. The symbol $\lfloor\cdot\rceil^{\alpha}$ is defined by $\lfloor\cdot\rceil^{\alpha} \triangleq \text{sign}(\cdot)|\cdot|^{\alpha}$.

Denote $e_{i,j,0} = \hat{x}_{i,j} - x_{i,j}$ and $e_{i,j,s} = z_{i,j,s} - \Delta_{i,j}^{(s-1)}$. From the interconnected (6) and the HOSM observer (7), one can obtain that the error dynamics gives

$$\begin{cases} \dot{e}_{i,j,0} = e_{i,j,1} - l_{i,j,0}\lambda_{i,j}^{\alpha_{i,j,0}} \lfloor e_{i,j,0} \rceil^{1-\alpha_{i,j,0}}, \\ \dot{e}_{i,j,s} = e_{i,j,s+1} - l_{i,j,s}\lambda_{i,j}^{\alpha_{i,j,s}} \lfloor e_{i,j,s} - \dot{e}_{i,j,s-1} \rceil^{1-\alpha_{i,j,s}}, \\ s \in \mathbb{N}_{1:n-j}, \\ \dot{e}_{i,j,n-j+1} = -\Delta_{i,j}^{(n-j)} - l_{i,j,n-j+1}\lambda_{i,j}^{\alpha_{i,j,n-j+1}}, \\ \qquad \times \lfloor e_{i,j,n-j+1} - \dot{e}_{i,j,n-j} \rceil^{1-\alpha_{i,j,n-j+1}}. \end{cases} \tag{8}$$

Secondly, noting that the tracking reference signal for $i-$th subsystem is y_{ri}, an auxiliary variable $\chi_{i,j}$ is declared by the following recursive steady state generators

$$\begin{cases} \chi_{i,1} = y_{ri}, \\ \chi_{i,j} = \frac{d\chi_{i,j-1}}{dt} - f_{i,j-1}(\bar{\chi}_{i,j-1}) - \Delta_{i,j-1}, \ j \in \mathbb{N}_{2:n+1} \end{cases} \tag{9}$$

where $\bar{\chi}_{i,j-1} \triangleq (\chi_{i,1}, \cdots, \chi_{i,j-1})^{\top}$.

Owing to the fact that $\Delta_{i,j-1}$ and its derivative terms are unaccessible in implementations, with the help of the HOSM observer (7), by replacing $\frac{d\Delta_{i,j}^{s}}{dt^s}$ by $z_{i,j,s+1}$ for $j \in \mathbb{N}_{1:n}$, $s \in \mathbb{N}_{0:n-j+1}$, we can obtain the following implementable variables

$$\begin{cases} x_{i,1}^* = y_{ri}, \\ x_{i,j}^* = \chi_{i,j}\big(z_{i,1,1}, \cdots, z_{i,1,j-1}, \cdots, z_{i,j-1,1}, \\ \qquad y_{ri}, y_{ri}^{(1)}, \cdots, y_{ri}^{(j-1)}\big), \ j \in \mathbb{N}_{2:n+1}. \end{cases}$$

Now, it enables to define a change of coordinates for subsystem i of the form

$$\xi_{i,j} = (x_{i,j} - x_{i,j}^*)/L^{j-1}, \ j \in \mathbb{N}_{1:n}, \ v_i = (u_i - x_{i,n+1}^*)/L^n$$

where $L \geq 1$ is a scaling gain to be made precise later. The interconnected system (6) equals to the following system

$$\begin{cases} \dot{\xi}_{i,j} = L\xi_{i+1} + (f_{i,j}(\bar{x}_{i,j}) - f_{i,j}(\bar{x}_{i,j}^*) + \omega_{i,j})/L^{j-1}, \\ j \in \mathbb{N}_{1:n-1}, \\ \dot{\xi}_{i,n} = Lv_i + (f_{i,n}(\bar{x}_{i,n}) - f_{i,n}(\bar{x}_{i,n}^*) + \omega_{i,n})/L^{n-1} \end{cases} \tag{10}$$

where $\bar{x}_{i,j}^* = (x_{i,1}^*, \cdots, x_{i,j}^*)^{\top}$, $j \in \mathbb{N}_{1:n}$, $\omega_{i,j} = f_{i,j}(\bar{x}_{i,j}^*) - f_i(\bar{\chi}_{i,j}) + x_{i,j+1}^* - \chi_{i,j+1} + \dot{\chi}_{i,j} - \dot{x}_{i,j}^*$.

Up to now, detaching from a recursive stability analysis procedure, a decentralized exact tracking control law of the following form could be straightforwardly built

$$u_i = L^n v_i + x_{i,n+1}^*, \ v_i = -\sum_{j=1}^{n} k_{i,j}\xi_{i,j}, \ i \in \mathbb{N}_{1:m} \tag{11}$$

where $K_i = [k_{i,1}, \cdots, k_{i,n}] \in \Re^{1\times n}$ is the decentralized control gain vector determined by a Hurwitz polynomial $p_i(s) = s^n + k_{i,n}s^{n-1} + \cdots + k_{i,2}s + k_{i,1}$.

Now we present the main theoretical result of this section whose rigourous proof is provided in the appendix.

Theorem 3.1: Consider the closed-loop system (6)-(7)-(11) in the sense that $x(0) \in \mho = [-\rho, \rho]^{nm}$ with $\rho \in \Re_+$ being a given constant which can be arbitrarily large. There exist sufficiently large parameters L and $\lambda_{i,j}$ for $i \in \mathbb{N}_{1:m}, j \in \mathbb{N}_{1:n}$, such that the following statements hold.

- i) All the trajectories of the closed-loop system are uniformly bounded.
- ii) The decentralized exact tracking can be realized, i.e., $\lim_{t\to\infty} y_i = y_{ri}, \ i \in \mathbb{N}_{1:m}$.

In addition to various existing decentralized control methods for interconnected systems, the proposed method has the following distinguishable features:

- Thanks to the HOSM observer, an exact decentralized tracking task can be achieved even the interconnected system is perturbed with mismatched disturbances and uncertain strongly coupled interactions.
- By utilizing a novel non-recursive design strategy, the design procedure could be largely simplified.
- It is also noted that the stability analysis can be essentially detached from the controller construction, which could facilitate the practical implementation.

IV. Controller Construction For DC Microgrids

Following the proposed control design procedure in the above section, we are now able to obtain a composite decentralized control scheme for each converter of the DC microgrid system. Detailed procedures are given below.

Firstly, we denote the following auxiliary functions

$$\begin{aligned} \chi_{i,1} &= 0.5L_i\Delta_{i,1}^2/E_i^2 + 0.5C_i v_{Cir}^2, \\ \chi_{i,2} &= \frac{d\chi_{i,1}}{dt} - \Delta_{i,1}, \\ \chi_{i,3} &= \frac{d\chi_{i,2}}{dt} - \Delta_{i,2}. \end{aligned} \tag{12}$$

Secondly, recalling that the load information R and P_{CPL} are clearly unaccessible, the following HOSM observers are hence required to online identify the lumped uncertainties:

$$1)\begin{cases}\dot{z}_{i,1,0}=x_{i,2}+\hbar_{i,1,0},\\ \dot{z}_{i,1,1}=\hbar_{i,1,1},\\ \dot{z}_{i,1,2}=\hbar_{i,1,2},\\ \dot{z}_{i,1,3}=\hbar_{i,1,3},\\ \hbar_{i,1,0}=-l_{i,1,0}\lambda_{i,1}^{1/4}\lfloor z_{i,1,0}-x_{i,1}\rceil^{3/4}+z_{i,1,1},\\ \hbar_{i,1,1}=-l_{i,1,1}\lambda_{i,1}^{1/3}\lfloor z_{i,1,1}-\hbar_{i,1,0}\rceil^{2/3}+z_{i,1,2},\\ \hbar_{i,1,2}=-l_{i,1,2}\lambda_{i,1}^{1/2}\lfloor z_{i,1,2}-\hbar_{i,1,1}\rceil^{1/2}+z_{i,1,3},\\ \hbar_{i,1,3}=-l_{i,1,3}\lambda_{i,1}\lfloor z_{i,1,3}-\hbar_{i,1,2}\rceil^{0};\end{cases}$$

$$2)\begin{cases}\dot{z}_{i,2,0}=u_i+\hbar_{i,2,0},\\ \dot{z}_{i,2,1}=\hbar_{i,2,1},\\ \dot{z}_{i,2,2}=\hbar_{i,2,2},\\ \hbar_{i,2,0}=-l_{i,2,0}\lambda_{i,2}^{1/3}\lfloor z_{i,2,0}-x_{i,2}\rceil^{2/3}+z_{i,2,1},\\ \hbar_{i,2,1}=-l_{i,2,1}\lambda_{i,2}^{1/2}\lfloor z_{i,2,1}-\hbar_{i,2,0}\rceil^{1/2}+z_{i,2,2},\\ \hbar_{i,2,2}=-l_{i,2,2}\lambda_{i,2}\lfloor z_{i,2,2}-\hbar_{i,2,1}\rceil^{0}.\end{cases}$$

Thirdly, by replacing the variables $\Delta_{i,1}, \Delta_{i,1}^{(1)}, \Delta_{i,1}^{(2)}, \Delta_{i,2}$ in $\chi_{i,j}$, $j=1,2,3$ with their corresponding estimates $z_{i,1,1}, z_{i,1,2}, z_{i,1,3}, z_{i,2,1}$, one can directly obtain the following steady-state function of each states as

$$\begin{aligned}x_{i,1}^*&=0.5L_iz_{i,1,1}^2/E_i^2+0.5C_i(V^*+m_iz_{i,1,1})^2,\\ x_{i,2}^*&=L_iz_{i,1,1}z_{i,1,2}/E_i^2+C_i(V^*+m_iz_{i,1,1})m_iz_{i,1,2}-z_{i,1,1},\\ x_{i,3}^*&=L_i(z_{i,1,2}^2+z_{i,1,1}z_{i,1,3})/E_i^2\\ &+C_i(V^*+m_iz_{i,1,1})m_iz_{i,1,3}+C_im_i^2z_{i,1,2}^2-z_{i,1,2}-z_{i,2,1}.\end{aligned}\tag{13}$$

With (13) in mind, using a change of coordinates:

$$\xi_{i,1}=x_{i,1}-x_{i,1}^*,\xi_{i,2}=(x_{i,2}-x_{i,2}^*)/L$$

where $L>1$ is a design parameter as denoted in Section III, the following decentralized composite controller for $i-$th converter could be explicitly constructed

$$u_i=-L^2\left(k_{i,1}\xi_{i,1}+k_{i,2}\xi_{i,2}\right)+x_{i,3}^*\tag{14}$$

where $k_{i,1}$, $k_{i,2}$ are control gains.

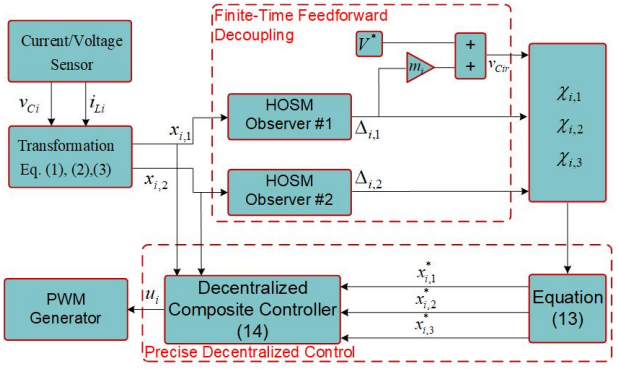

Fig. 2: Control architecture of the proposed controller.

According to the above design philosophy, the control architecture of the proposed controller for the droop control is shown by Fig. 2. Meanwhile, the control architecture of classical double-loop PI controller is also provided in Fig. 3 to present a visualized comparison. It can be clearly observed that by utilizing a double-layer integrated feedforward compensation loop, the proposed composite control strategy is enabled to achieve an immediate reaction to the variation of system operating condition. Hence a fast performance recovery ability as well as a large signal stability could both be guaranteed.

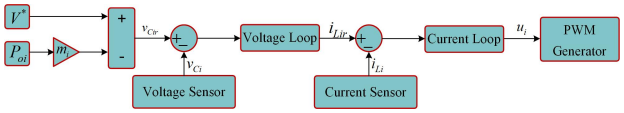

Fig. 3: Control architecture of the classical double-loop PI controller.

It is worth pointing out that even a higher-order observer would provide a more delicate estimation, but in the mean time, a trade-off issue is its weakened robustness against sensor error and measurement noise. Noting that in DC systems, the uncertainty terms $\Delta_{i,1}$, $\Delta_{i,2}$ are physically slow time-varying signals, which admit smaller derivatives with an increasing order. Hence in the implementations, the order of HOSM observers could also be practically reduced for the sake of less sensitivity to measurement noises.

V. Simulation Results and Discussions

To validate the proposed control strategy, simulation tests are conducted in Matlab/Simulink. The classical double closed-loop PI controller is chosen to compare with the proposed controller so as to manifest the superiorities of the proposed method. Detailed parameters are provided in Table I. For the sake of fair comparison, it is noted that the benchmark PI control gain parameters are well selected according to reference [14], [25] in order to meet an optimal control performance.

Table I. System Parameters Configuration

Parameters	Description	Value
V^*	nominal bus voltage	170V
E_1, E_2	converter input voltage	100V
L_1, L_2	nominal inductance value	2mH
C_1, C_2	nominal capacitance value	470uF
$l_{i,1,s}, s=0,1,2,3$	observer gains for observer #1	5, 4, 2, 1
$l_{i,2,s}, s=0,1,2$	observer gains for observer #2	4, 2, 1
$\lambda_{i,j}$	observer scaling gains $(i,j=1,2)$	1e9
$k_{i,1}, k_{i,2}$	controller gains $(i=1,2)$	30, 20
L	controller scaling gain	100
f_{sw}	switching frequency	20kHz
k_{cp}, k_{ci}	PI gains for current control loop	0.13, 35
k_{vp}, k_{vi}	PI gains for voltage control loop	0.3, 35

Case 1. Tuning of Design Parameters: The selection and evaluation of the parameters for both HOSM observer and controller are conducted in the first section. Given the fact that both the objective of constant voltage mode and droop mode is to track the reference voltage v_{Cir}, i.e., the parameters of any mode can be utilized in another mode without any changes. Hence, only the performances of the constant voltage mode is investigated in this subsection to avoid the redundancy of this paper.

Table II. Simulation Performances Between Proposed Controller and PI Controller.

Controllers	Variations	Inductor current		Bus voltage	
		Transient time(ms)	Maximum deviation(A)	Transient time(ms)	Maximum deviation(V)
Proposed	Input voltage: 100V → 80V	12	0.075	15	0.102
	Input voltage: 100V → 60V	25	0.154	30	0.203
	CPL: 200W → 400W → 200W	7	0.231	7	0.458
	CPL: 200W → 800W → 200W	12	1.077	10	2.500
PI	Input voltage: 100V → 80V	100	0.202	40	0.632
	Input voltage: 100V → 60V	173	0.462	50	1.405
	CPL: 200W → 400W → 200W	38	0.385	43	1.958
	CPL: 200W → 800W → 200W	40	1.000	42	5.41

Firstly, according to HOSM observer #1, the output power observation with different observer gains (λ_i=1e7, 1e8, 1e9, 1e10, 1e11) under the control scaling gain (L_i=100) are shown in Fig. 4. With the CPL changes from 100W to 200W, all of the observers with different gains can accurately track the changes of load. But the difference is that the increased λ_i leads to a faster convergence ability. As can be observed from Fig. 4, the duration of transient process is only 1ms with the λ_i=1e11. But meanwhile, it lasts 23ms when the observer gain is set as 1e7. Although in our methodology, the design produce of the observer and controller can be separately done. However, it stands to reason that the improved performances of the observer will lift the properties of the controller, which is well illustrated in Fig. 6. As the observer gains increase, the observer can estimate the changes of load and send the obtained value to the controller more quickly. The DC bus voltage reaches to its desirable value in 4ms with λ_i being selected as 1e11. In contrast, a long duration of 25ms can be observed when it is set as 1e7.

Secondly, the controller scaling gain L_i is further adjusted to expect a better performance. As is shown in Fig. 6, the voltage regulation performances are recorded under a series of L_i settings (60, 80, 100, 120, 140) while λ_i is fixed at 1e9. It is evident from this figure that the transient process can be greatly shorten by increasing L_i. However, it should be pointed out that it is inadvisable to blindly pursue quick response characteristics especially considering the application of real power electronic systems.

From the above simulation results and analysis, the parameters of λ_i and L_i are finally determined as 1e9 and 100 respectively.

Case 2. Input Voltage Variation Test: In this case, the converter input voltage is changed to examine the stabilization performance. Two DU subsystems are involved and their droop coefficients are both set as 0.01. At the beginning, the bus voltage is regulated at 167.7V and a 450W CPL is connected to the DC bus. As 0.3s, the converter input voltage of DU1 steps down from 100V to 80V and DU2 remains unchanged. In order to guarantee the rated output power according to the previous settings, DU1 has to release additional current to compensate the power resulting from the voltage drop. As is shown in Fig. 7, DU1 controlled by the proposed approach responses immediately and reaches to its desired value quickly. Owing to its preeminent transient characteristics, DU2 can be immune to this sudden change and keeps constant current output. In contrast, DU1 controlled by the PI controller spends almost 100ms to achieve the desired value. Hence, the current fluctuation occurs until the current of DU1 achieves its desired value. The performance on bus voltage in Fig. 8 also reflects the differences between two candidate controllers. It is not difficult to find that the recovery capability of bus voltage gets markedly promoted under the proposed control strategy. Soon after, the same type of comparison continues while the changes of the input voltage are doubled. Similar to the previous case, the proposed controller maintains its consistent quick property. Both the current and voltage can be stabilized within a short time. In the mean time, a longer response time and a large current/voltage deviation can be observed under the PI controller. Relevant simulation results are shown in Figs. 9 and 10.

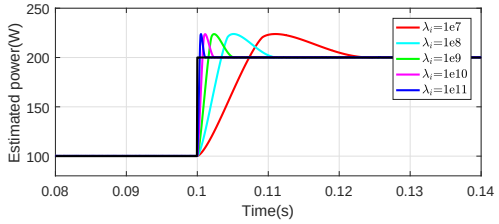

Fig. 4: Load estimation responses with different values of λ_i.

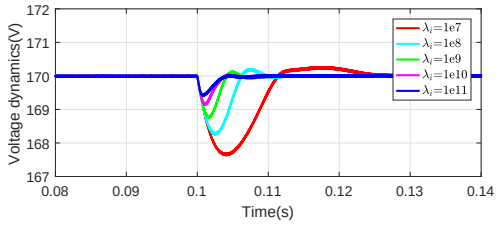

Fig. 5: Voltage dynamic responses with different values of λ_i.

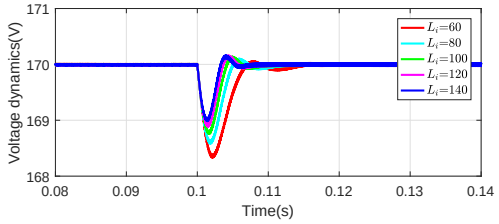

Fig. 6: Voltage dynamic responses with different values of L_i.

Case 3. CPL Variation Test: The CPL is changed in this case to further explore the advantages which have brought by the proposed control method. The basic setting is identical with the former case. Initially, the bus voltage is stable at 169V and a 200W CPL is connected. Then, the CPL increases to 400W in 0.25s and decreases to 200W in 0.45s. The transient response of bus voltage is shown in Fig. 12. With the same load change, obvious voltage overshoot can be observed under the PI controller. The amplitude of the voltage overshoot goes down by 2.2V and the duration of the recovery process is 30ms. Meanwhile, the proposed controller demonstrates excellent dynamic performance consistently. Upon the disturbances happen, the proposed controller can adjust its operating voltage and reach a steady state in a short period of time. Besides, by further looking into the current output shown in Fig. 11, the proposed strategy not only shows fast dynamic performance as always, but also realizes the accurate power sharing as we set before. In the following case, a wider range of variation magnitudes is tested to compare the two alternative controllers. Distinguished from the previous case, the CPL in this case goes straight up to 800W in 0.25s and turns back to 200W in 0.45s. As plotted in Fig. 13, an obvious current overshoot can be observed in both proposed and PI controller due to the enormous variation in operating conditions. Nevertheless, the proposed controller still performs better than the PI controller both in rapid recovery of voltage and precise regulation of current. The comparisons results between proposed controller and PI controller are summarized in Table II, which provides a visual representation of two controllers.

Case 4. Plug-and-Play Property Test: In what follows, the PnP property is tested under both the proposed controller and PI controller. DU3 is introduced in this case and its basic setting is identical with previous DUs. As is shown in Fig. 15, three DUs are considered in this test, whose droop coefficients are set as 0.01, 0.02 and 0.015, respectively. At first, DU1 and DU3 work together to supply 750W CPL. Meanwhile, DU2 operates independently with 200W CPL. At 0.2s, another 250W CPL is added into the double DU system and the power of DU1 and DU3 increases to 600W and 400W (3:2). In order to take the load off of the DU1 and DU3, DU2 is connected to the DC bus at 0.3s. The power is reallocated according to their respective droop coefficients, that is 553W, 369W, 278W (6:3:4). Subsequently, the 250W CPL is removed at 0.4s and the output power of each DU decreases to 438W, 220W, 292W (6:3:4). At 0.5s, DU3 is disconnected. The bus voltage response curve is shown in Fig. 15(c). The above tests prove the plug-and-play property of the proposed strategy is well built. It should be pointed out here that the PI parameters employed in previous cases achieve poor performances. In order to present a fair comparison, the PI parameters for voltage and current loop ($k_{vp}, k_{vi}, k_{ip}, k_{ii}$) are selected as 0.3, 40, 0.08 and 50. Nonetheless, the performances of PI controller cannot compare with its competitor, for example, when the CPL is increased by 250W, about 5V voltage drop can be observed in Fig. 16(c). Then, DU3 joins in the coordinated control at 0.3s and all of three DUs change the output power slowly. Not until they fully achieve their rated output value, the CPL is reduced by 250W and the voltage overshoot occurs again. Similar performances can also be observed at 0.5s and the voltage does not always switch smoothly.

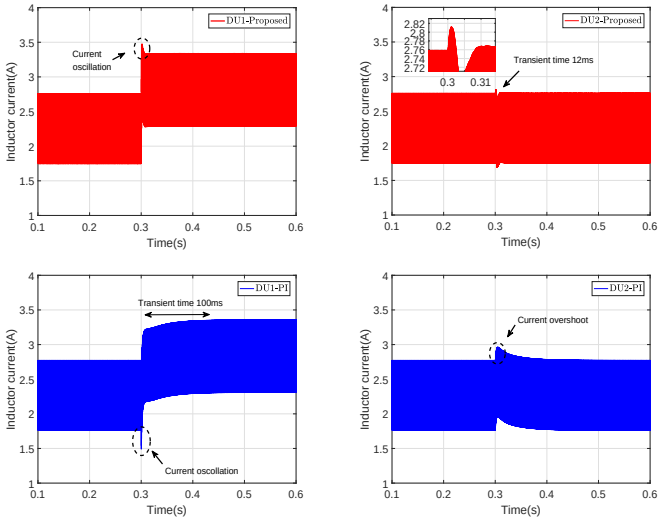

Fig. 7: Current responses with a converter input voltage variation from 100V to 80V.

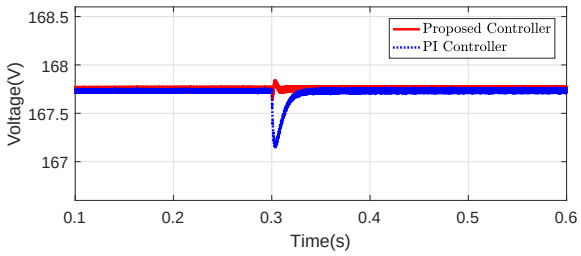

Fig. 8: Bus voltage responses with a converter input voltage from 100V to 80V.

VI. Experimental Tests and Comparison Study

In order to verify the proposed decentralized control strategy, a small-scale DC microgrid experimental platform, which is shown in Fig. 17, has been studied. The platform consists of two programmable DC power supplies, two DC-DC boost converters, a dSPACE 1006 controller, a resistive load and an electronic load. The control algorithms are executed on dSPACE to generate PWM signals for two converters. To examine the stability of the system, the programmable electronic load operates in constant power mode to emulate the CPL. In the meantime, the DC microgrid is operated in the droop mode and the droop coefficients of DU1 and DU2 are set as 0.01. For the sake of less sensitivity to measurement noise, the observers are both selected as third order. The parameters of converter components are identical with Table II while the gain parameters $l_{i,j,0}$, $l_{i,j,1}$, $l_{i,j,2}$, $\lambda_{i,j}$, L, $k_{i,1}$, $k_{i,2}$ are redesigned as 200, 400, 200, 10, 650, 1, 2 for optimal practical control performance.

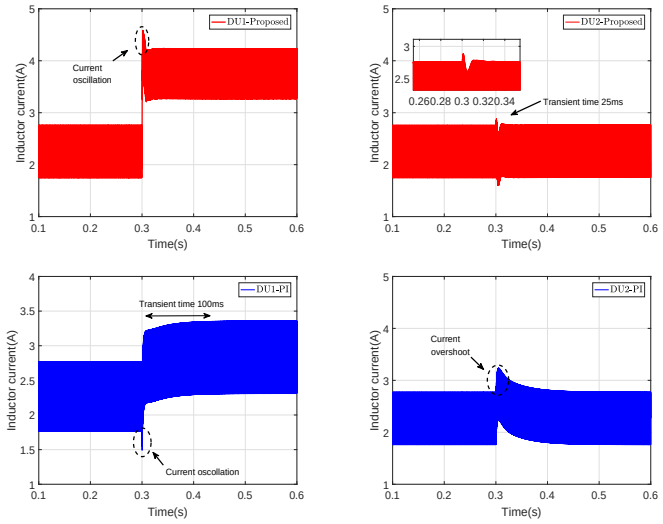

Fig. 9: Current responses with a converter input voltage variation from 100V to 60V.

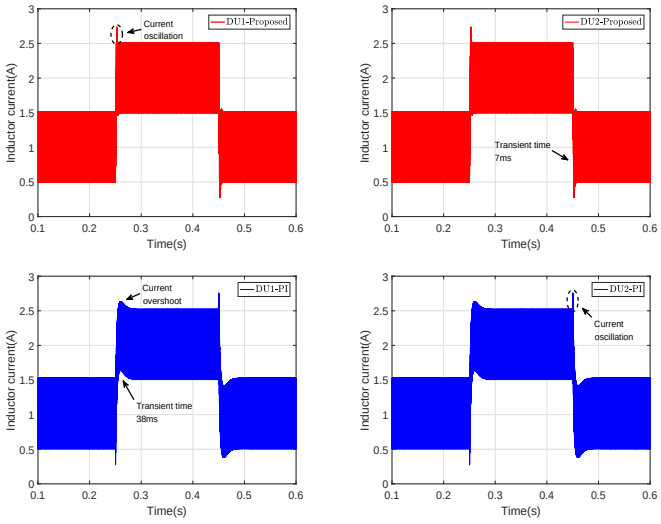

Fig. 11: Current responses with load variations from 200W to 400W, and from 400W to 200W.

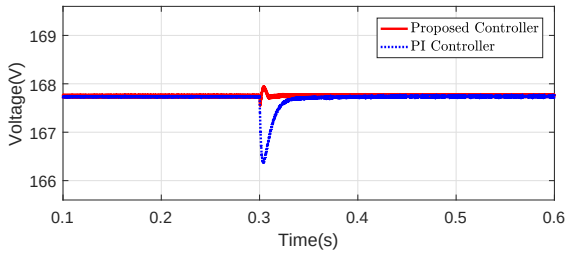

Fig. 10: Bus voltage responses with a converter input voltage from 100V to 60V.

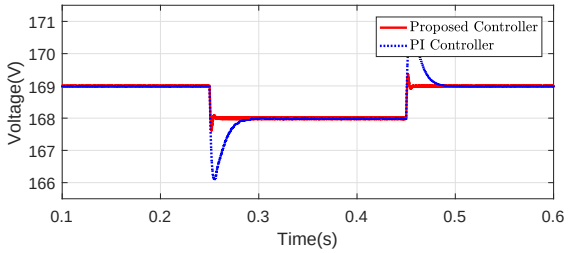

Fig. 12: Bus voltage responses with load variations from 200W to 400W, and from 400W to 200W.

In what follows, experimental results are provided to verify the proposed control strategy. The input voltage changes and the variations of the loads are both considered in the experimental studies.

Firstly, the converter input voltage is changed to examine the stabilization issue of the system. DC bus is rigorously regulated at 167.7V and a 650Ω resistive load is connected to the DC bus. As shown in Fig. 18, the converter input voltage of DU1 steps down from 100V to 80V and DU2 remains unchanged. In order to keep the constant voltage of the DC bus, the current amplitude of DU1 rises from 2.25A to 2.8A in a short period of time. It can be observed that both candidate controllers could achieve similar performances, which is beneficial from the effort we spent in tuning the parameters for both controllers, aiming for a fair control performance comparison in the subsequent cases.

Secondly, only CPL is connected to the DC bus in order to test the microgrid system stability under different variation conditions of the CPL. Fig. 19 shows the experimental results when the CPL steps up from 50W to 650W. It demonstrates that in this case, the PI controller can also achieve the control objective and maintain system stability. Thereafter, to compare the stability margin and outstand the advantages of the proposed controller, as shown in Fig. 20, a larger CPL variation case is conducted when the CPL suddenly changes from 50W to 1100W. Although the voltage has a slight drop, the proposed controller is able to maintain the stability of the DC bus at 154.5V eventually. With regard to the PI controller under the same control parameters setup as in the former cases, it is obvious that large oscillation occurs and increases until the system collapses. Consequently, it is confident to reach that the proposed controller is able to stabilize the system towards a large-signal stability, and therefore provides a wider operating range for DC microgrid system.

VII. CONCLUSION

Accurate power sharing and decentralized control for DC microgrids in a large-signal stability sense are of critical significance. To this end, we explicitly design a novel decentralized composite controller by integrating an alternative finite-time performance recovery process. With the expression of a simple linear controller form, the proposed design strategy could also lead to an easy practical implementation. It is illustrated by numerical simulation and experimental tests that a faster transient-time response as well as a larger stability margin are both achieved compared with the classical double-loop PI

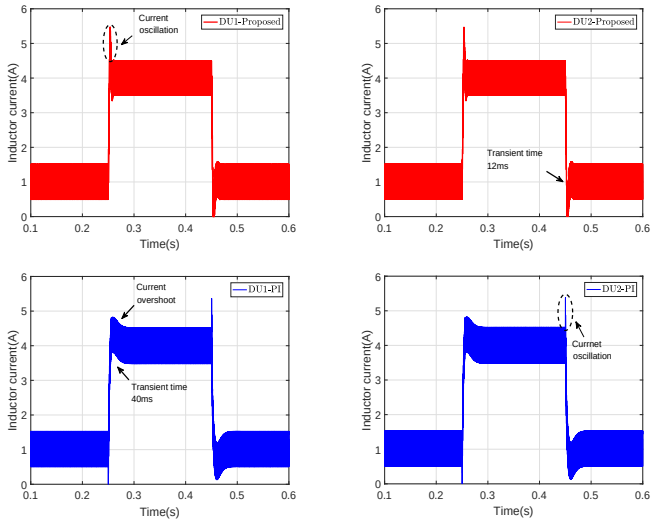

Fig. 13: Current responses with load variations from 200W to 800W, and from 800W to 200W.

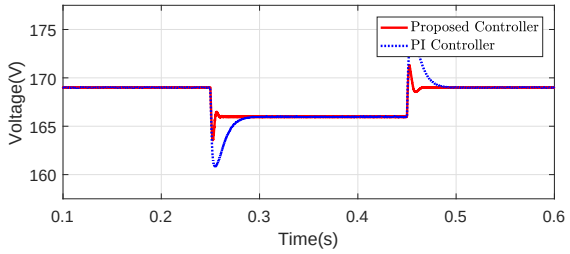

Fig. 14: Bus voltage responses with load variations from 200W to 800W, and from 800W to 200W.

controller. Future works may focus on optimal and adaptive control design under the basis of large-signal stabilization.

APPENDIX

Proof of Theorem 3.1: Denote $A_i \in \Re^{n\times n}, B_i \in \Re^{n\times 1}$ be two matrices of the controllability canonical form, $F_i(\cdot) \triangleq [(f_{i,1}(\bar{x}_{i,1}) - f_{i,1}(\bar{x}^*_{i,1}))/L^0, (f_{i,2}(\bar{x}_{i,2}) - f_{i,2}(\bar{x}^*_{i,2}))/L^1, \cdots, (f_{i,n}(\bar{x}_{i,n}) - f_{i,n}(\bar{x}^*_{i,n}))/L^{n-1}]^\top$ and $\tilde{\omega}_i = [\omega_{i,1}/L^0, \omega_{i,2}/L^1, \cdots, \omega_{i,n}/L^{n-1}]^\top$. System (10) can also be rewritten as the following compact form

$$\dot{\xi}_i = L(A_i\xi_i + B_i v_i) + F_i(\cdot) + \tilde{\omega}_i,\ i \in \mathbb{N}_{1:m}. \tag{15}$$

By further defining $v = [v_1, \cdots, v_m]^\top$, $\xi = [\xi_1^\top, \cdots, \xi_m^\top]^\top$ $F = [F_1^\top, \cdots, F_m^\top]^\top$, $\tilde{\omega} = [\tilde{\omega}_1^\top, \cdots, \tilde{\omega}_m^\top]^\top$, and $\Lambda = \text{diag}\{A_1 - B_1K_1, \cdots, A_m - B_mK_m\}$, one can obtain the compact form for system (15) under the decentralized control law (11) with $i \in \mathbb{N}_{1:m}$ as follows

$$\dot{\xi} = L\Lambda\xi + F(\cdot) + \tilde{\omega}. \tag{16}$$

In this step, by noting that Λ is a Hurwitz matrix, hence we can construct a positive definite, proper Lyapunov function of the form $V(\xi) = \xi^T P\xi$, where $P \in \Re^{nm}$ is a positive definite and symmetrical matrix satisfying $\Lambda^T P + P\Lambda = -I$.

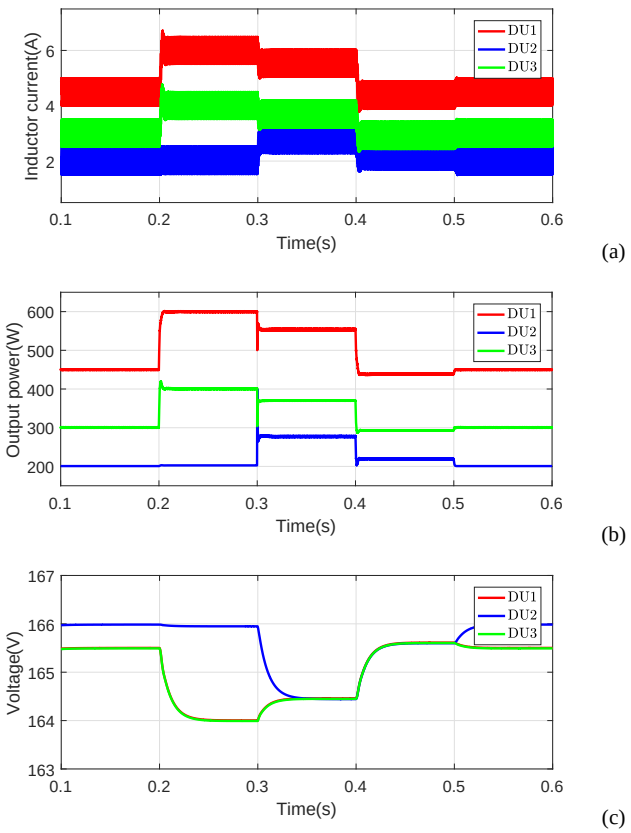

Fig. 15: Performances of PnP test for proposed controller, (a) current responses, (b) power responses, (c) voltage responses.

Calculating the time derivative along system (16) gives

$$\dot{V}(\xi) = \frac{\partial V(\xi)}{\partial \xi^\top} L\Lambda\xi + \frac{\partial V(\xi)}{\partial \xi^\top} F(\cdot) + \frac{\partial V(\xi)}{\partial \xi^\top}\tilde{\omega}. \tag{17}$$

i) In what follows, under the controller (11), we shall prove that any trajectory satisfying $x(0) \in \mho \triangleq [-\rho, \rho]^{nm}$ can be rendered uniformly bounded. If this claim is not true, assume there exists an escape time $T_f < \infty$, that is, $x(t)$ is well defined on the maximally extended interval $[0, T_f)$ and moreover, $\lim_{t\to T_f} \|x(t)\| = +\infty$.

Now we consider the time interval $[0, T_f)$. Note that $\Delta_{i,j} \in \mathcal{C}^{n-j+1}$ and $|\Delta_{i,j}^{(n-j)}| \le \mathcal{D}_{i,j}$. Assume the observer gain $\lambda_{i,j}$ satisfies $\sup\{|\Delta_{i,j}^{(n-j)}|\} \le \mathcal{D}_{i,j}$. From [24], we know that all signals in (8) should be uniformly bounded on $[0, T_f)$. This fact also implies that $x^*_{i,j}$, $\omega_{i,j}$ are bounded on $[0, T_f)$, i.e., $\max_{i\in\mathbb{N}_{1:m}, j\in\mathbb{N}_{1:n}} \{\sup\{|x^*_{i,j}|\}\} \le \bar{\rho}$, $\max_{i\in\mathbb{N}_{1:m}, j\in\mathbb{N}_{1:n}} \{\sup\{|\omega^*_{i,j}|\}\} \le \tilde{\rho}$ where $\bar{\rho} \in \Re_+$ and $\tilde{\rho} \in \Re_+$ are constants.

Based on the above discussion, we are able to define a level set as $\Omega = \{\xi \in \Re^{nm} | V(\xi) \le \rho_0,\ \rho_0 = \max_{\xi\in[-(\rho+\bar{\rho}),\rho+\bar{\rho}]^{nm}} \{V(\xi)\}\}$.

On the one hand, noticing the fact that $f_{i,j} \in \mathcal{C}^\infty$ and $L \ge 1$, by Mean-Value Theorem, the following inequalities can be

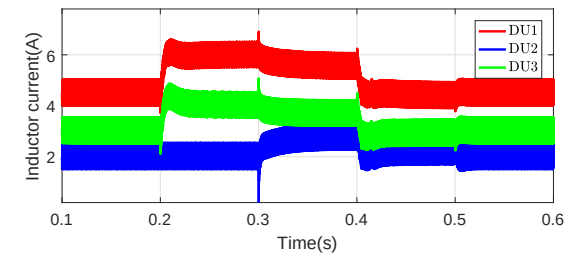

(a)

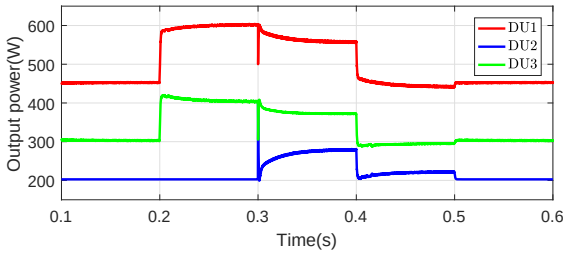

(b)

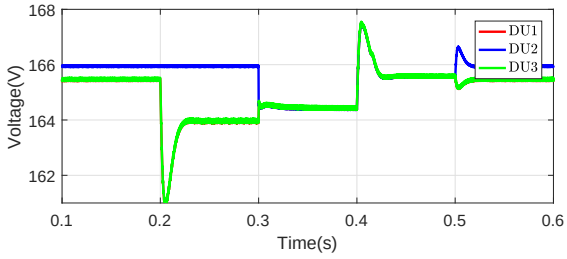

(c)

Fig. 16: Performances of PnP test for PI controller, (a) current responses, (b) power responses, (c) voltage responses.

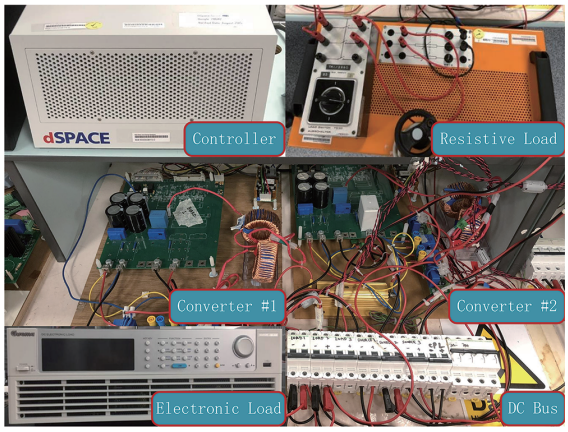

Fig. 17: Experiment Setup.

easily obtained

$$\begin{aligned}
&\frac{f_{i,j}(\bar{x}_{i,j}) - f_{i,j}(\bar{x}^*_{i,j})}{L^{j-1}} \\
&\le \frac{\gamma_{i,j}}{L^{j-1}}\Big(|x_{i,1} - x^*_{i,1}| + |x_{i,2} - x^*_{i,2}| + \cdots + |x_{i,j} - x^*_{i,j}|\Big) \\
&\le \gamma_{i,j}\Big(|\xi_{i,1}|/L^{j-1} + |\xi_{i,2}|/L^{j-2} + \cdots + |\xi_{i,j}|/L^{j-j}\Big) \\
&\le \gamma_{i,j}\Big(|\xi_{i,1}| + |\xi_{i,2}| + \cdots + |\xi_{i,j}|\Big), \ \text{for } \xi \in \Omega, \qquad (18)
\end{aligned}$$

where $\gamma_{i,j}$ is a constant which is dependent on Ω but independent of L. Then, with (18) in mind, one will further have

$$\begin{aligned}
&\frac{\partial V(\xi)}{\partial \xi^T} F(\cdot)\big|_{\Omega} \\
&= \sum_{i=1}^{m}\sum_{j=1}^{n} \frac{\partial V(\xi)}{\partial \xi_{i,j}} (f_{i,j}(\bar{x}_{i,j}) - f_{i,j}(\bar{x}^*_{i,j}))/L^{j-1} \\
&\le \sum_{i=1}^{m}\sum_{j=1}^{n} \left|\frac{\partial V(\xi)}{\partial \xi_{i,j}}\right| \gamma_{i,j}\Big(|\xi_{i,1}| + |\xi_{i,2}| + \cdots + |\xi_{i,j}|\Big) \\
&\le c\|\xi\|^2 \qquad (19)
\end{aligned}$$

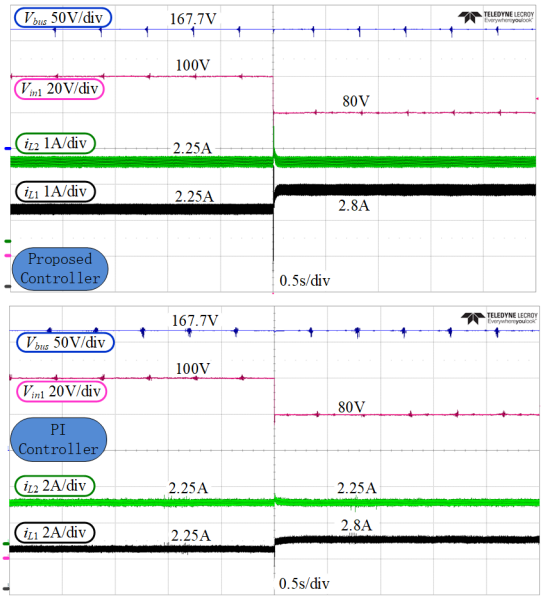

Fig. 18: Experimental comparison results with a converter input voltage variation from 100V to 80V.

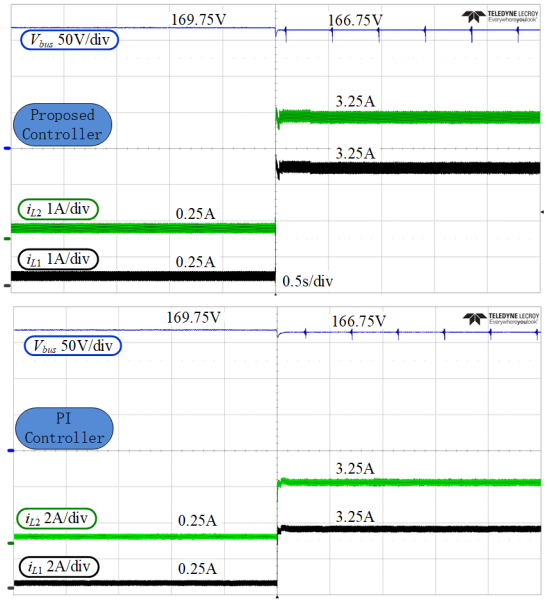

Fig. 19: Experimental comparison results with a CPL variation from 50W to 650W.

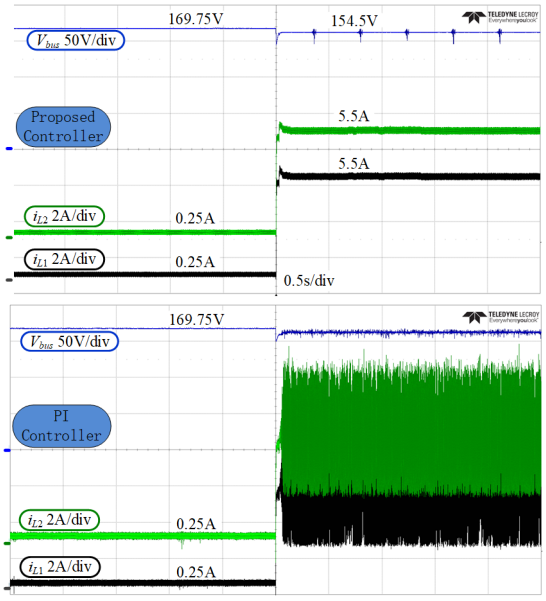

Fig. 20: Experimental comparison results with a large CPL variation from 50W to 1100W.

where $c \in \Re_+$ is a constant.

On the other hand, by using the completion of squares, the following relations hold on $[0, T_f)$

$$\begin{aligned}\frac{\partial V(\xi)}{\partial \xi^T}\tilde{\omega} &\leq 2\lambda_{\max}(P)\|\xi\|\|\tilde{\omega}\| \\ &\leq \bar{c}\|\xi\|^2 + \tilde{c}\|\tilde{\omega}\|^2 \\ &\leq \bar{c}\|\xi\|^2 + \Gamma \end{aligned} \tag{20}$$

where $\bar{c} \in \Re_+, \tilde{c} \in \Re_+$ and $\Gamma \geq \tilde{c}nm\tilde{\rho}^2$ are all constants.

By substituting (19) and (20) into (17), it yields

$$\dot{V}(\xi)\big|_{\mathbf{\Omega}} \leq -(L - c - \bar{c})\|\xi\|^2 + \Gamma, \ t \in [0, T_f). \tag{21}$$

Now the selection guideline of L can be explicitly given as

$$L \geq c + \bar{c} + \max\{1, 2\Gamma\lambda_{\max}(P)/\rho_0\}. \tag{22}$$

Recalling the claim that the trajectory of $\xi(t)$ must escape the level set Ω within a finite time smaller than T_f. Owing to the fact that $\xi(0) \in \Omega$, there must exists a time instant T_s satisfying $T_f > T_s > 0$, such that the following relations hold

$$a)\ V(\xi(T_s)) = \rho_0;\ b)\ \dot{V}(\xi(T_s)) > 0. \tag{23}$$

Clearly, the relation (21) still holds for $t \in [0, T_s]$, which together with (22) implies

$$\begin{aligned}\dot{V}(\xi(T_s)) &= -(L - c - \bar{c})\|\xi\|^2 + \Gamma \\ &\leq -(L - c - \bar{c})V(\xi(T_s))/\lambda_{\max}(P) \\ &\quad + \frac{1}{2}(L - c - \bar{c})\rho_0/\lambda_{\max}(P) \\ &\leq -\frac{1}{2}\rho_0/\lambda_{\max}(P) < 0 \end{aligned} \tag{24}$$

which clearly contradicts the claim $b)$ of (23). Hence we know that under the guideline (22), the trajectory of $\xi(t)$ will stay in Ω forever, that is, $x(t)$ is well defined on $[0, \infty)$.

ii) Now we come back to the error dynamics (8). By following [24], we know there exists a finite time, denoted by T, such that $e^s_{i,j}(t) = 0,\ t \geq T$ for $i \in \mathbb{N}_{1:m},\ j \in \mathbb{N}_{1:n},\ s \in \mathbb{N}_{0:n-j+1}$.

Hence, the following relation can be achieved

$$\dot{V}(\xi)\big|_{\Omega} \leq -(L - c - \bar{c})\|\xi\|^2,\ t \in [T, \infty). \tag{25}$$

Based on the guideline (22), it implies straightforwardly that $\lim_{t\to\infty} y_i = y_{ri},\ i \in \mathbb{N}_{1:m}$. This completes the proof of Theorem 3.1.

REFERENCES

[1] P. Savage, R. R. Nordhaus, and S. P. Jamieson, "DC microgrids: Benefits and barriers," *From Silos to Systems: Issues in Clean Energy and Climate Change*, pp. 51–66, 2010.

[2] M. Kabalan, P. Singh, and D. Niebur, "Large signal lyapunov-based stability studies in microgrids: A review," *IEEE Transactions on Smart Grid*, vol. 8, no. 5, pp. 2287–2295, 2017.

[3] A. Emadi, A. Khaligh, C. H. Rivetta, and G. A. Williamson, "Constant power loads and negative impedance instability in automotive systems: definition, modeling, stability, and control of power electronic converters and motor drives," *IEEE Transactions on Vehicular Technology*, vol. 55, no. 4, pp. 1112–1125, 2006.

[4] E. Hossain, R. Perez, A. Nasiri, and S. Padmanaban, "A comprehensive review on constant power loads compensation techniques," *IEEE Access*, vol. 6, pp. 33285–33305, 2018.

[5] "IEEE Recommended Practice for Electronic Power Subsystems: Parameters, Interfaces, Elements, and Performance," *IEEE Standard*, pp. 1573–2003, 2004.

[6] T. Dragičević, X. Lu, J. C. Vasquez, and J. M. Guerrero, "DC microgrids: Part i: A review of control strategies and stabilization techniques," *IEEE Transactions on Power Electronics*, vol. 31, no. 7, pp. 4876–4891, 2016.

[7] S. Anand and B. Fernandes, "Reduced-order model and stability analysis of low-voltage dc microgrid," *IEEE Transactions on Industrial Electronics*, vol. 60, no. 11, pp. 5040–5049, 2013.

[8] L. Guo, S. Zhang, X. Li, Y. W. Li, C. Wang, and Y. Feng, "Stability analysis and damping enhancement based on frequency-dependent virtual impedance for dc microgrids," *IEEE Journal of Emerging and Selected Topics in Power Electronics*, vol. 5, no. 1, pp. 338–350, 2017.

[9] M. Su, Z. Liu, Y. Sun, H. Han, and X. Hou, "Stability analysis and stabilization methods of dc microgrid with multiple parallel-connected dc–dc converters loaded by CPLs," *IEEE Transactions on Smart Grid*, vol. 9, no. 1, pp. 132–142, 2018.

[10] Q. Xu, C. Zhang, C. Wen, and P. Wang, "A novel composite nonlinear controller for stabilization of constant power load in dc microgrid," *IEEE Transactions on Smart Grid*, vol. 10, no. 1, pp. 752–761, 2019.

[11] P. Lin, C. Zhang, P. Wang, and J. Xiao, "A decentralized composite controller for unified voltage control with global system large-signal stability in dc microgrids," *IEEE Transactions on Smart Grid, in press*, 2018.

[12] P. Magne, D. Marx, B. Nahid-Mobarakeh, and S. Pierfederici, "Large-signal stabilization of a dc-link supplying a constant power load using a virtual capacitor: Impact on the domain of attraction," *IEEE Transactions on Industry Applications*, vol. 48, no. 3, pp. 878–887, 2012.

[13] S. Sanchez and M. Molinas, "Large signal stability analysis at the common coupling point of a dc microgrid: A grid impedance estimation approach based on a recursive method," *IEEE Transactions on Energy Conversion*, vol. 30, no. 1, pp. 122–131, 2015.

[14] S. Bacha, I. Munteanu, and A. I. Bratcu, "Power electronic converters modeling and control," *Springer London*, 2014.

[15] L. Bakule, "Decentralized control: status and outlook," *Annual Reviews in Control*, vol. 38, no. 1, pp. 71–80, 2014.

[16] D. Šiljak, "Decentralized control and computations: status and prospects," *Annual Reviews in Control*, vol. 20, pp. 131–141, 1996.

[17] J. T. Feddema, C. Lewis, and D. A. Schoenwald, "Decentralized control of cooperative robotic vehicles: theory and application," *IEEE Transactions on Robotics and Automation*, vol. 18, no. 5, pp. 852–864, 2002.

[18] C. Wen and J. Zhou, "Decentralized adaptive stabilization in the presence of unknown backlash-like hysteresis," *Automatica*, vol. 43, no. 3, pp. 426–440, 2007.

[19] C. Wen, J. Zhou, and W. Wang, "Decentralized adaptive backstepping stabilization of interconnected systems with dynamic input and output interactions," *Automatica*, vol. 45, no. 1, pp. 55–67, 2009.
[20] X. Zhang and Y. Lin, "Nonlinear decentralized control of large-scale systems with strong interconnections," *Automatica*, vol. 50, no. 9, pp. 2419–2423, 2014.
[21] C. Zhang, C. Wen, and L. Wang, "Nonsmooth decentralized stabilization for interconnected systems subject to strongly coupled uncertain interactions," *IEEE Transactions on Systems, Man, and Cybernetics: Systems, in press*, 2018.
[22] S. Li, J. Yang, W. Chen, and X. Chen, *Disturbance Observer-Based Control: Methods and Applications*. CRC Press, 2014.
[23] C. Zhang, Y. Yan, C. Wen, J. Yang, and H. Yu, "A nonsmooth composite control design framework for nonlinear systems with mismatched disturbances: Algorithms and experimental tests," *IEEE Transactions on Industrial Electronics*, vol. 65, no. 11, pp. 8828–8839, 2018.
[24] A. Levant, "Higher-order sliding modes, differentiation and output-feedback control," *International Journal of Control*, vol. 76, no. 9-10, pp. 924–941, 2003.
[25] P. Lin, P. Wang, J. Xiao, J. Wang, C. Jin, and Y. Tang, "An integral droop for transient power allocation and output impedance shaping of hybrid energy storage system in dc microgrid," *IEEE Transactions on Power Electronics*, vol. 33, no. 7, pp. 6262–6277, 2018.

Chuanlin Zhang (M'14) received the B.S. degree in mathematics and the Ph.D. degree in control theory and control engineering from the School of Automation, Southeast University, Nanjing, China, in 2008 and 2014, respectively. He was a Visiting Ph.D. Student with the Department of Electrical and Computer Engineering, University of Texas at San Antonio, USA, from 2011 to 2012; a Visiting Scholar with the Energy Research Institute, Nanyang Technological University, Singapore, from 2016 to 2017; a visiting scholar with Advanced Robotics Center, National University of Singapore, from 2017 to 2018. Since 2014, he has been with the College of Automation Engineering, Shanghai University of Electric Power, Shanghai, where he is currently a Professor and the director of Intelligent Autonomous Systems Laboratory.

He is the principal investigator of several research projects, including Eastern Scholar Program at Shanghai, Leading Talent Program of Shanghai Science and Technology Commission, Chenguang Program by the Shanghai Municipal Education Commission, etc. His research interests include nonlinear system control theory and applications for power systems.

Xiaoyu Wang (S'19) was born in Yancheng, Jiangsu Province, China in 1995. He received the B. Sc degree in electrical engineering from North China Electric Power University Science & Technology College in 2017. He is currently working toward M. Sc degree with the College of Automation Engineering, Shanghai University of Electric Power, China.

He is a member of Intelligent Autonomous Systems Laboratory , under the guidance of Prof. C. Zhang. His research interests include DC microgrids stability and control.

Pengfeng Lin (S'16) received the B.Sc. and M.Sc. degree in electrical engineering from Southwest Jiaotong University, China, in 2013 and 2015 respectively. He is currently working toward Ph.D degree in Interdisciplinary Graduate School, Eri@n, Nanyang Technological University, Singapore. His research interests include energy storage systems, hybrid AC/DC microgrids and electrical power system stability analyses.

Peter Xiaoping Liu (F'19) received his B.Sc. and M.Sc. degrees from Northern Jiaotong University, China in 1992 and 1995, respectively, and Ph.D. degree from University of Alberta, Canada in 2002. He has been with the Department of Systems and Computer Engineering, Carleton University, Canada since July 2002 and he is currently a Professor and Canada Research Professor. His interest includes interactive networked systems and teleoperation, haptics, surgical simulation, robotics, control and intelligent systems. Dr. Liu has served as an Associate Editor for several journals including IEEE/ASME Transactions on Mechatronics, IEEE Transactions on Cybernetics, IEEE Transactions on Automation Science and Engineering, and IEEE Transactions on Instrumentation and Measurement. He is a licensed member of the Professional Engineers of Ontario (P.Eng), a Fellow of the Engineering Institute of Canada (FEIC) and a Fellow of IEEE (FIEEE).

Yunda Yan (S'15-M'18) received the B.Sc degree from School of Automation in Southeast University, Nanjing, China in 2013. He is currently working toward the Ph.D. degree in control theory and control engineering from School of Automation in Southeast University under the guidance of Profs. Shihua Li and Jun Yang. He was a visiting student at Department of Biomedical Engineering, National University of Singapore under the guidance of Prof. Haoyong Yu from Oct. 2016 to Oct. 2017; and was a visiting student at Department of Aeronautical and Automotive Engineering, Loughborough University under the guidance of Dr. Cunjia Liu and Prof. Wen-Hua Chen from Dec. 2017 to Dec. 2018.

His current research interests include the development of predictive control methods, dynamic high-gain control methods, control allocation methods and disturbance modeling and estimation approaches and their applications in motion control systems.

Jun Yang (SM'18) received the B.Sc. degree from the Department of Automatic Control, Northeastern University, Shenyang, China, in 2006, and the Ph.D. degree in control theory and control engineering from the School of Automation, Southeast University, Nanjing, China, in 2011. He is currently a Professor with the School of Automation, Southeast University.

His current research interests include disturbance estimation and compensation, advanced control theory, and its application to flight control systems and motion control systems. Dr. Yang is an Associate Editor of the TRANSACTIONS OF THE INSTITUTE OF MEASUREMENT AND CONTROL. He recieved the ICI prize for best paper of TRANSACTIONS OF THE INSTITUTE OF MEASUREMENT AND CONTROL in 2016.